

Post-collapse analysis of Morandi's Polcevera viaduct in Genoa Italy

*Original*

Post-collapse analysis of Morandi's Polcevera viaduct in Genoa Italy / Morgese, M.; Ansari, F.; Domaneschi, M.; Cimellaro, G. P.. - In: JOURNAL OF CIVIL STRUCTURAL HEALTH MONITORING. - ISSN 2190-5452. - STAMPA. - 10:(2020), pp. 69-85. [10.1007/s13349-019-00370-7]

*Availability:*

This version is available at: 11583/2818042 since: 2020-04-30T18:46:43Z

*Publisher:*

Springer

*Published*

DOI:10.1007/s13349-019-00370-7

*Terms of use:*

This article is made available under terms and conditions as specified in the corresponding bibliographic description in the repository

*Publisher copyright*

(Article begins on next page)

# Post Collapse Analysis of Morandi's Polcevera Viaduct in Genoa Italy

Maurizio Morgese <sup>a</sup>, Farhad Ansari <sup>b</sup>, Marco Domaneschi <sup>c</sup>, and Gian Paolo Cimellaro <sup>d</sup>

<sup>a</sup> PhD Student, Dept. of Civil and Materials Engineering, University of Illinois at Chicago, Illinois, USA, Email: mmorg3@uic.edu

<sup>b</sup> Professor, Dept. of Civil and Materials Engineering, University of Illinois at Chicago, Illinois, USA, (Corresponding author) Email: fansari@uic.edu

<sup>c</sup> Assistant Professor, Dept. of Structural, Geotechnical and Building Engineering, Politecnico di Torino, Italy, Email: marco.domaneschi@polito.it

<sup>d</sup> Associate Professor, Dept. of Structural, Geotechnical and Building Engineering, Politecnico di Torino, Italy, Email: gianpaolo.cimellaro@polito.it

## Abstract

Morandi's Polcevera viaduct was an important transportation link that connected port of Genoa to other major cities in Europe. The bridge was in service for over fifty years and carried the traffic over one of the busiest highways in Europe. Real time structural health monitoring would have provided data for maintenance and warned of impending failure. The objective of the study reported herein, was to estimate the remaining service life and predicting the end of life for the bridge in the absence of available sensor data. The analysis involved time-domain estimation of bridge capacity loss over the period of bridge service and increase in demand over the same period. In addition to the existing information about the bridge, combined effects of corrosion and fatigue were considered in estimating the decrease in the capacity of the bridge from the time it was placed in service. Classical influence line analysis of the individual sections of the pylon-deck system of the bridge, together with the finite element model of the bridge provided the numerical tool for analysis of the bridge. A number of different approaches were compared in estimating the

remaining life of the bridge, including the cumulative damage law of Palmgren and Miner, as well as the Goodman, Gerber and Soderberg mean fatigue stress diagrams. The predicted timing of collapse by these models ranged from the year 2014 based on the cumulative damage law, and 2016 by the Gerber and Goodman diagrams. The estimates from this study predict the collapse of the bridge 2-4 years prior to the actual collapse date in 2018. The results of this study indicated that even without an active instrumented structural health monitoring system, basic engineering principles may provide the backing for estimation of remaining life of the infrastructure. In the case of the Morandi bridge, such an analysis at some point during its service life, would have possibly predicted imminence of collapse prior to the actual collapse.

**Keywords:** Morandi Bridge; Polcevera viaduct; Fatigue; Corrosion; Collapse, Bridge, Truck loads; Palmgren-Miner law; Goodman diagram; Greber diagram Soderberg diagram

## **1. Introduction**

The Polcevera viaduct in Genoa, Italy, commonly referred to after its designer Riccardo Morandi, partially collapsed on August 14, 2018 killing 43 people. The construction of the bridge was completed in 1967, and its collapse after 51 years of service was a reminder of the poor state of infrastructure and condition of the mid twentieth century bridges. In fact, 115 major bridge collapses have occurred around the globe since the year 2000, and over twenty-two of them occurred in the past two years. Some of the bridge collapses in the recent history were due to natural or man-made hazards, i.e. in earthquakes, mud slides, floods, and accidents, and some others were related to construction site related errors, such as in early removal of support structures. However, in general, a majority of collapses occur while the bridges are in-service, and during their normal operational settings. Collapse of Morandi's Polcevera viaduct falls into this latter category. At the time of this writing, the official investigation into the failure of the Morandi bridge was still ongoing. It is however useful to review some of the collapses of the recent past considering their significance, and their corollary with the failure of Polcevera viaduct. Post collapse investigation reports from many of these bridges reveal that in most cases, the progression of events leading to the collapses follow similar patterns. Generally, catastrophic failures involve a combination of several bridge-condition-related issues, which are triggered by failure of a weakened element of the bridge [1, 2].

A notable example is the 1967 collapse of the Silver Bridge, which set the precedence for mandatory biennial inspection of bridges in USA. The Silver Bridge, an eyebar suspension bridge, put to service in 1928, spanned over the Ohio River and connected the states of Ohio and West Virginia. The bridge collapsed in December of 1967 during the rush hour traffic, causing the deaths of 46 people [3]. The bridge was 39 years in service at the time of collapse. Post collapse investigation of the bridge revealed that the failure of a single eyebar due to a 0.1-inch-deep corrosion-induced defect triggered the failure [4]. In addition, the bridge lacked redundancy, and the investigation also showed that the bridge was subjected to heavier loads than it was designed for, poorly maintained, and it was not inspected since 1951.

The 2007 catastrophic collapse of the I-35W Bridge in Minneapolis, Minnesota serves as another example. The bridge was placed in service in 1967. It was designed as a continuous truss-arched bridge with a total length of 581 meters, and a width of 34.1 meters. Its longest span was 139 meters in length carrying 140,000 vehicles across the Mississippi River. The bridge collapse occurred during the rush-hour traffic. It involved 117 vehicles, killed 13 individuals, and injured 145 motorists. The bridge had received the condition rating of “poor” in 1991, and 2006, respectively [5]. The findings of inspectors following the 2006 inspection revealed deficiencies such as poor weld details, corrosion, connections sway, faded paint, surface rust; and section loss in various elements, such as in main truss members, floor beams, cross beams and in rocker bearings [6]. The field investigation reports, as well as structural analysis of the bridge indicated that the failure initiated at a pair of 13 -mm thick gusset plates, which were not thick enough to provide sufficient capacity for the stress demands at the section. The gusset plates were made of ASTM A441 grade 50 steel connecting five truss members with 25 mm diameter rivets [7].

The 1994 collapse of the Seongsu bridge in South Korea, as well as the 1983 collapse of Mianus River bridge in Connecticut are other examples. The Seongsu bridge was placed in service in 1979, and it was 1150-meter-long crossing the Han river. The failure was triggered by weld failure in the trusses of the suspension structure causing the collapse of the concrete slab killing 32 people with a number of injuries [8]. The 1983 collapse of Mianus River bridge, in Greenwich, Connecticut involved three fatalities. The original bridge a multi-span girder and floor beam structure was built in 1958. The investigation by the National Transportation Safety Board indicated that rusting of the bearing pin started a fatigue crack causing the collapse of a 100 feet

section of the deck [9]. Issues cited in the report ranged from lack of inspection, inadequate drainage, fracture critical bearings and lack of redundancy.

Comprehensive review of recent bridge collapses is beyond the scope of the present article. More case studies can be found elsewhere [10, 11]. Interestingly, most of the failed bridges were built in the mid twentieth century and in service for 40 years or more prior to failure. Their state of health was poor, with signs of corrosion, fatigue cracks, and in some cases, hidden design flaws. The designs lacked redundancy, and in most cases with fracture critical elements, whose failure would probably cause a portion of or the entire bridge to collapse. With population growth and expansion of global economy over the recent decades the failed bridges were subjected to steady increase in traffic volume and heavy axle weights. More importantly, these bridges were not maintained in consistent manner and their condition was not regularly assessed. Systematic monitoring of these major bridges would have provided warnings about impending failures [12], such as unusual strain increases in gusset plates, unstable fatigue crack growth [13], loss of cable tension [14], and others.

Genoa is an important industrial hub, and a major port in Northern Italy. Morandi Bridge was a road viaduct on the A10 motorway in Genoa. A10 motorway connects to the French A8 autoroute, and forms part of European route E80. It is one of the busiest highways in Italy, with constant truck traffic carrying freight between Italy and the rest of the Europe. The bridge was located within few kilometers of large factories, including steel plants with airborne emissions (Fig.1). The bridge was only 2.4 kilometers away from the Mediterranean Sea, with direct exposure to sea salt aerosol. At the time of collapse, the bridge had been in service for over 50 years. The prestressed concrete cables were not properly maintained and showed signs of corrosion. The bridge lacked redundancy and its prestressed concrete cables on the three pylons of the bridge were considered fracture critical.

In most countries, bridges are usually designed for a service life of 75 years, and in addition to biennial inspections (i.e. in USA), they generally receive an overhaul by mid-life [15]. In the case of the Morandi bridge, one of the three pylons, P11 in Fig. 3, was repaired in 1992, by replacing its corroded cables with new sets of cables. The rest of the pylons did not receive any repairs, which eventually one of them, P9 in Fig. 3, failed and instigated the partial collapse of the bridge [16, 17].



**Figure 1:** Proximity of the Polcevera viaduct to the main sources of corrosive emissions: the sea and an industrial hub



**Figure 2.** Pitting corrosion of prestressing tendons.

Following the failure of Polcevera viaduct, some considered the influence of bad weather and lightning on the collapse. However, degradation of the cables due to corrosion was confirmed by an investigation carried out by the inspection commission of the Ministry of Infrastructure and

Transport (MIT) [16, 17]. Fig. 2 pertains to a photo of the corroded tendons, taken by Autostrade, which is the operating entity for the highway system that includes the Polcevera viaduct.

The objective for the study reported herein was to determine whether it was possible to predict the failure or the collapse of this bridge or similar bridges, or to estimate the remaining service life, in lieu of sensor based structural health monitoring. Considering the amount of forensic information available at the time of writing this article, the work presented in this article is based on the hypothesis that the collapse of the bridge occurred due to a combination of fatigue and corrosion of the cables. In testing the hypothesis, the work presented in this article pertains to the study that involve in-service estimation of structural demand as well as the capacity of the bridge. Realistic estimation of demand and capacity require information about the condition history of the bridge, local environment, and traffic, especially in terms of truck loads. Moreover, it is also necessary to have information about specific design and construction features of the structure, and post collapse forensic investigation reports. Considering lack of sensor based structural health monitoring data, the methodology presented herein aims at providing a realistic estimate of actual lifespan of a bridge. However, the post collapse analysis of the bridge in this study is based on selection and use of available tendon corrosion models found in the technical literature, and extrapolation of traffic data. Hence, selection of one corrosion model or the other, and or a different approach in estimating the evolution of truck traffic loads over the service life of the bridge would have altered the results of the analysis. Considering the uncertainties, careful estimation of the bridge loads based on the available data, and selection of appropriate corrosion models, as well as, realistic analysis of the structure enables reasonable estimates of remaining service life. Background information about the Polcevera viaduct is provided next, followed by the description of the approach, numerical simulations, and the results.

## **2. Unusual Features of the Polcevera Viaduct**

Polcevera viaduct or the Morandi bridge was designed and built by Riccardo Morandi. The construction of the infrastructure began in 1963, and the bridge was placed in service in 1967 [18, 19]. The viaduct includes three cable-stayed system, each supported a three-span continuous beam by two sets of prestressed concrete cables on the two sides of the pylon across the width. On each side of the pylon the cables ran over a saddle to reach the other side of the continuous beam. The three sets of continuous beams were connected together by buffer beams with Gerber saddles [18,

19]. The bridge deck was made of a partially prestressed concrete slab. The pylons of the bridge formed a double V, one to support the deck beam and the other, which was an upside-down V to support the stays over the saddle. The schematic diagram of the bridge and details for a typical pylon-girder assembly as well as the Gerber beam connecting the three sections are shown in Fig. 3.

In general, cable-stayed bridges are designed to possess several stays. They fan out from the pylons and support the deck at several locations, distributing and balancing the loads along the deck [20 – 22]. The design of cable stays at Morandi Bridge was different, and only had two stays per each pylon. This together with the saddle seats at the top of the pylons for running the cable from one side to the other (Fig. 4), made it impossible for the bridge to remain intact if one cable snapped. Moreover, instead of steel cables, the tendons at the Morandi bridge were made of prestressed concrete, making it difficult to inspect the tendons. The corrosive effects of the Mediterranean air and the airborne pollution from the steel mills contributed to removal of superficial chemical resistance of concrete, paving the path to the corrosion aggression [23, 24].

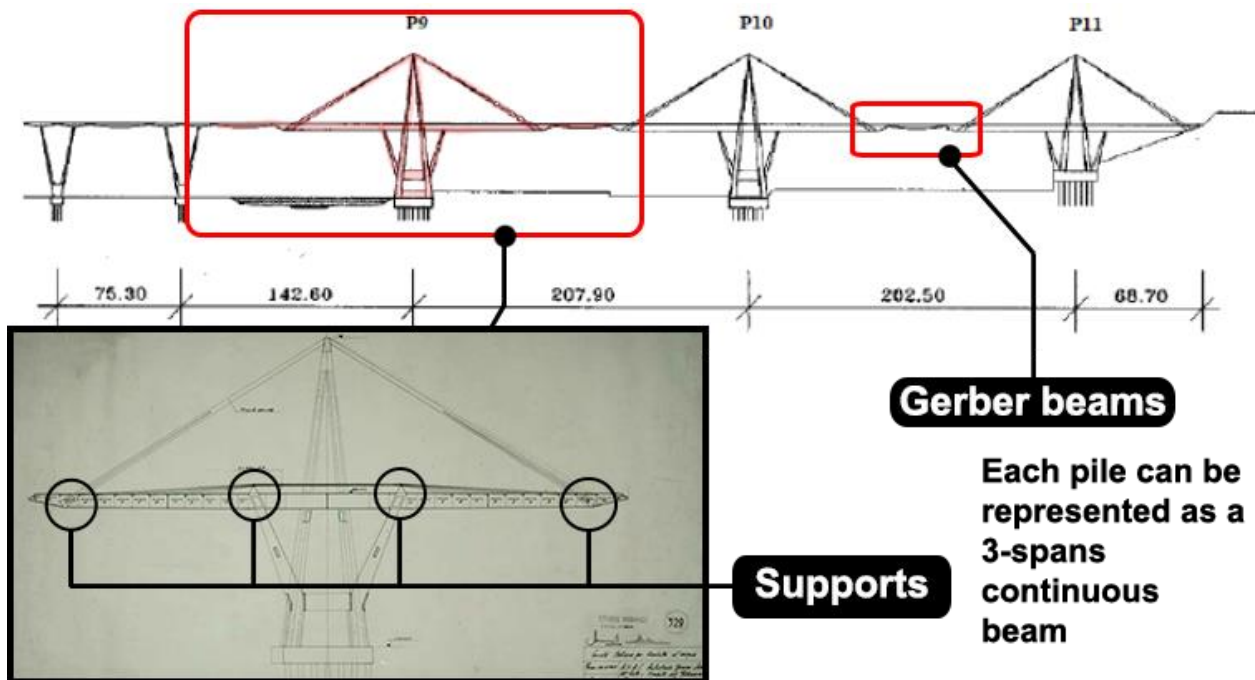


**Figure 3.** Schematic diagram of the Polcevera Viaduct.



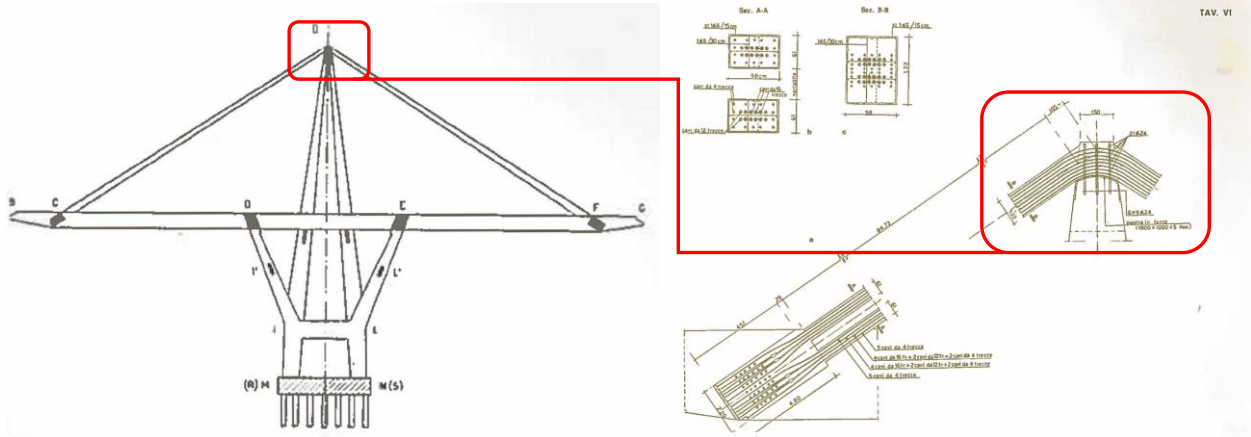


**Figure 4.** Typical view of the stay cable system with the saddle detail from the design tables.

### 3. Construction of the bridge

Construction of the bridge took place in five phases, which are enumerated in the following, and depicted in Fig.5 [18, 19]:

1. The pylons were constructed first, consisting of two V-shaped elements, one of them an inverted V. The V-shaped elements were connected together by transverse beams at top and mid-height, and at the base to the foundation.
2. The deck was constructed in segments extending from pylons and temporarily held in position by an external post tensioned cable.
3. At the completion of Phase 2, steel tendons (Cables-A) were connected to the deck extremities by transverse beams. These cables were continuously crossed over the top of the pylon through a saddle. At the completion of this stage, the temporary cables were removed. Once this phase of the construction was completed, the dead loads were routed to four supports, consisting of two internal transverse braces, and two cables (Cables-A).
4. Phase 4 involved completion of the entire system by addition of cables-B [18, 19]. At this stage concrete formwork was constructed around Cables-A, and then the formwork was filled with concrete and post tensioned by tendons (Cables-B). In addition, the ducts containing cables-B were required to be injected with grout. During this operation, the concrete formwork and Cables-B were not connected to the deck in order to maintain the original equilibrium of the system under dead loads. Therefore, the concrete casing was

under full compression due to the above-mentioned post tensioning processes. The final segment of this phase involved connecting the prestressed concrete stays to the deck girders.

5. Phase 5 involved construction of the simply supported transfer (Gerber) beams, which were employed for connecting the three sets of deck-pylon structures.

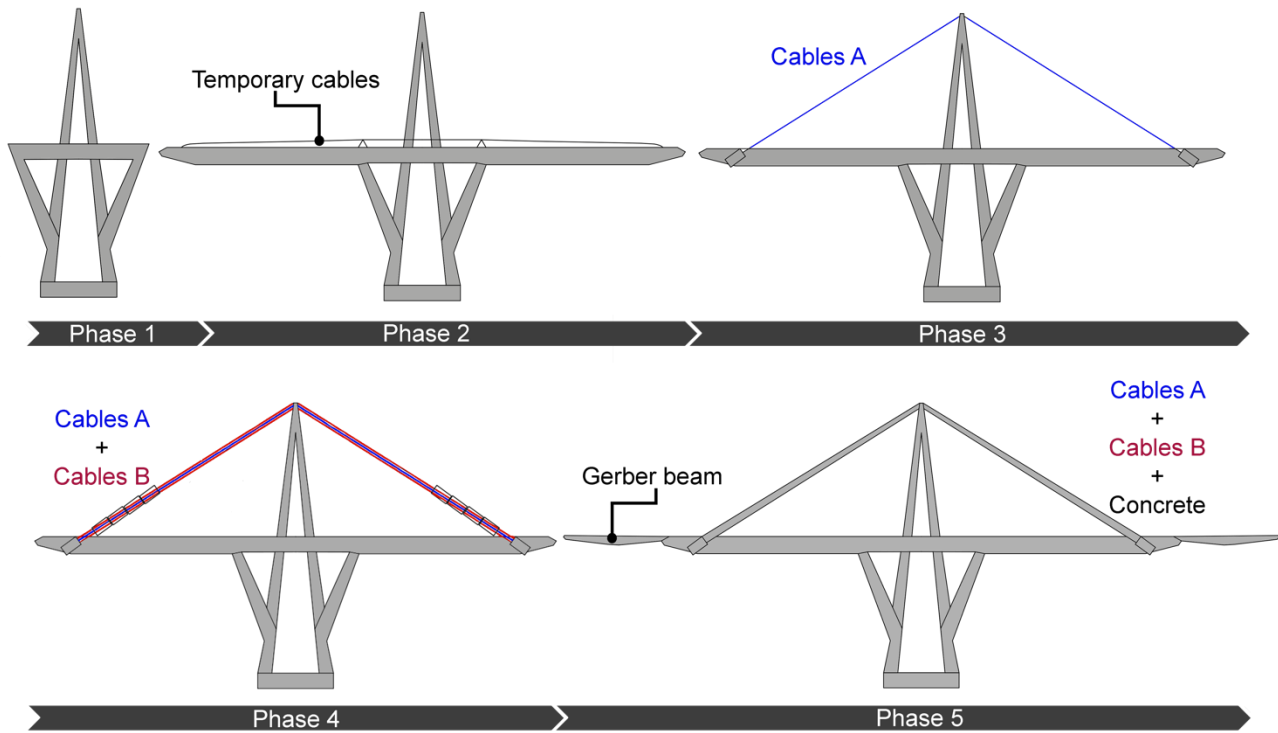


**Figure 5.** Construction phases of Polcevera Viaduct.

The prestressing tendon details within the cross-sections of the cable stays are shown in the photo of a typical deck-pylon structure of the bridge in Fig.6. The two different cross-sections portray the transition of the stay cable from a single cross-section on the upper portion of the stay on both sides of the saddle to double sections in the lower region, at the connecting points to the bridge deck. The larger single cross section around the saddle was necessary in order to assure smooth transition over the highly concentrated stresses at the saddle. Division of the cross section at the deck was necessary to spread the effect of the concentrated force. Despite the transition, the cross-sectional area and the number of prestressing tendons within each cross-section remained the same (Fig.6). The inner cables (Cables-A), which were installed during phase-3 of the construction

comprised of 24 tendons, each tendon with 12 strands for a total of 288 strands per cable. The external cables (Cables-B), were comprised of 28 tendons, each with 4 strands for a total of 112 strands. A typical tendon pattern signifying the positions of cables-A and B is shown in Fig. 7.

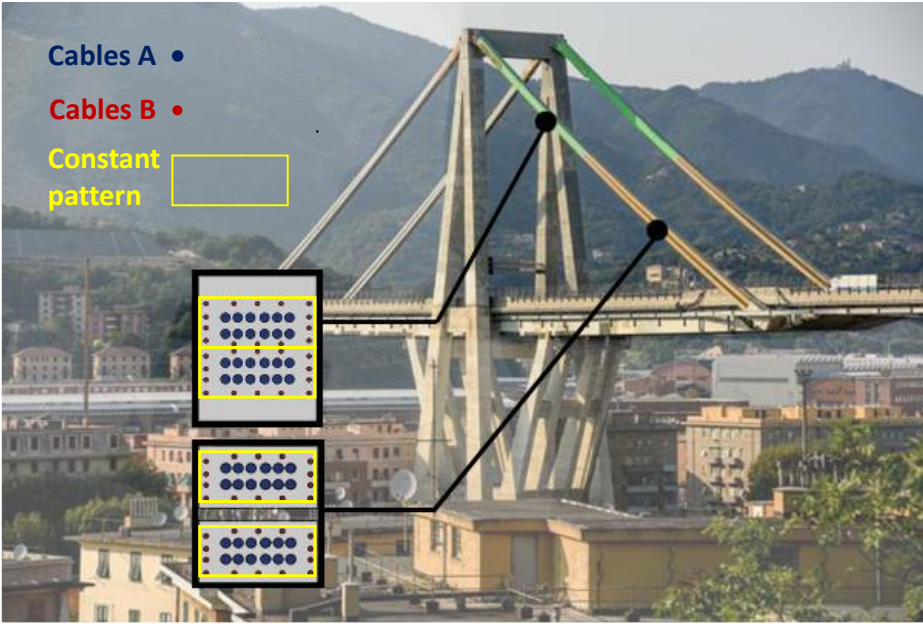


**Figure 6.** Cross-sections of the stays at Polcevera Viaduct

With reference to construction phases, the intent was to assure support for the main deck dead loads by Tendons A and compression of the concrete stay cover by Tendons B. Both cable types contributed in supporting the Gerber beams (Phase 5) and the live loads.

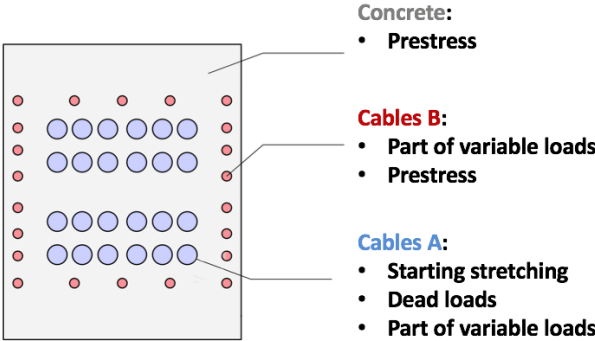


**Figure 7.** Load configuration per Morandi's design specifications for the stays

It is also noted that Morandi used prestressed concrete, as opposed to steel cables, in order to reduce the difference between the stiffnesses of stays and the deck. He also intended to protect the stays against corrosion by using the concrete as a barrier. However, the original plan for injection of grout in the ducts during phase 4 of the operations was not successful [18, 19]. Many segments within the ducts were not fully filled with the grout materials. Issues pertaining to the inefficiency of manual injection pumps due to the diagonal orientation of the formwork at the bridge site, and limited void diameter in the tendon ducts for efficient delivery of grout were cited as a reason for unsuccessful grout injection operations [25]. Consequently, in the official investigation by the ministry of infrastructure and transportation (2018), the deficiency of grout in the tendon ducts was considered the main culprit for instigating pitting corrosion in the steel tendons.

#### **4. Post Collapse Analysis Scheme**

The proposed methodology for the analysis of collapse involves time-domain estimation of bridge capacity loss over the period of bridge service and increase in demand over the same period (1968 – 2018). Fig. 8 is a flowchart providing the overall capacity-demand process for post collapse analysis of the Morandi Bridge. Precursors to the analysis were the facts that: (1) the bridge lacked redundancy; (2) its design possessed unusual features, i.e. concrete cables and the saddles; and (3) the cables were not regularly inspected and or maintained, except for P11 in Fig. 3, which was replaced in 1992 as described earlier. Considering these precursors, the process follows linear analysis, both in terms of yearly decrease in capacity and increase in demand, respectively. The increase in demand was due to both the volume of traffic and the magnitude of truck axle loads over the last 50 years in Europe, and the increase in container ship and cruise ship traffic at the port of Genoa.

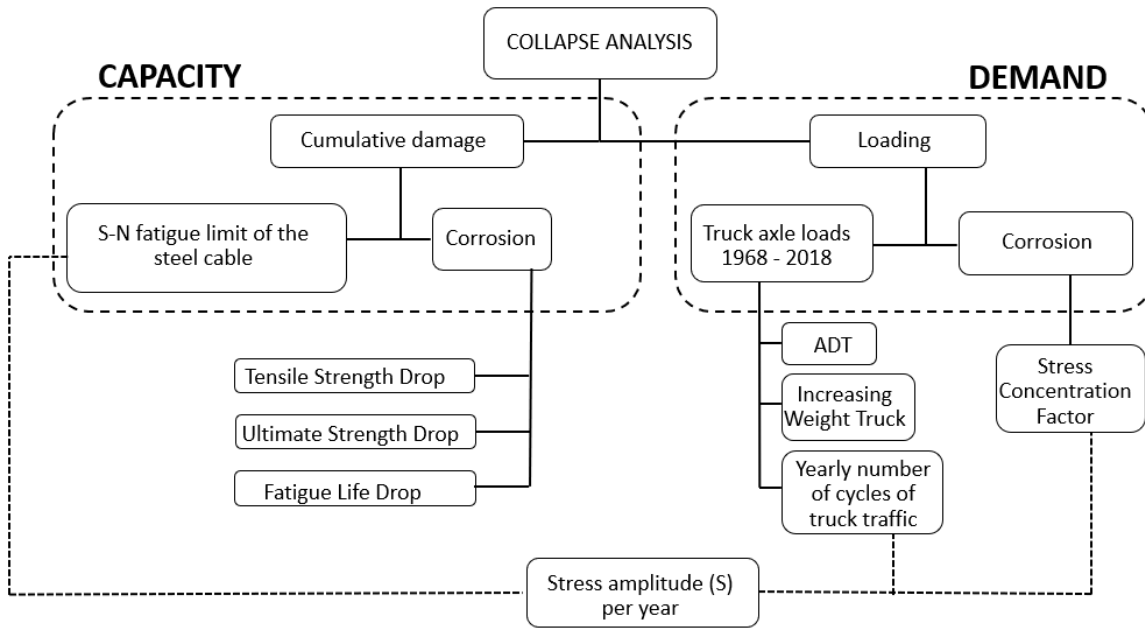


**Figure 8.** Flow diagram for the analysis of capacity and demand of the Polcevera Viaduct

Based on the general processes depicted in Fig. 8, post collapse analysis of the bridge requires realistic portrayal of degradation (corrosion and fatigue) and loads over the period of its service life. For estimation of capacity loss due to corrosion and fatigue, the first step in the process involved survey of technical literature for the selection of appropriate models. On the other hand, computation of demand required estimation of loads on the bridge. In addition to the self-weight as the dead load, truck traffic information was employed for the computation of the live loads. Live loads were computed as a representative set of truck axle loads typical of trucks in the Italian design standard guidelines. The number of passenger cars travelling over the bridge increased over the years. However, contribution of passenger cars to the loads were not considered in the post collapse analysis. This was a conservative assumption for the post collapse analysis. A model was also necessary to compute the corrosion related stress changes in the bridge elements over the period of its service. Once sufficient amounts of data and information became available, it was then possible to use the original design drawings of the Morandi bridge for development of a detailed 3D finite element model of the pylon-deck system (P9 in Fig. 3). Influence lines were also computed in order to identify the maximum effect of truck axle loads on internal forces at critical members. Computation of demand and capacity was repeated for each year of service until the

failure of the most critical component of the bridge. Details pertaining to the implementation of the proposed approach are described in the following sections of this article.

## 5. Bridge Loading

The load combination for post collapse analysis of the bridge composed of both dead loads and live loads. Dead loads were computed based on the weights of structural elements from the original design drawings of the bridge and the estimated weight of the wearing surface on the deck. Accurate portrayal of the live loads was important considering their importance both in design as well as for estimating the effects of fatigue on the degradation of the bridge [26]. In the context of present study, database from the Italian Association of Motorways and Tunnel Operators, AISCAT [27] was employed for the estimation of truck traffic over the Morandi bridge. It was possible to extract the traffic data from the AISCAT's database, covering the period between 1968 and 2018. As shown in Fig. 9, the number of trucks traveling over the bridge (Average Daily Traffic, ADT) increased from 3,885 in 1968 to 24,640 in 2018.

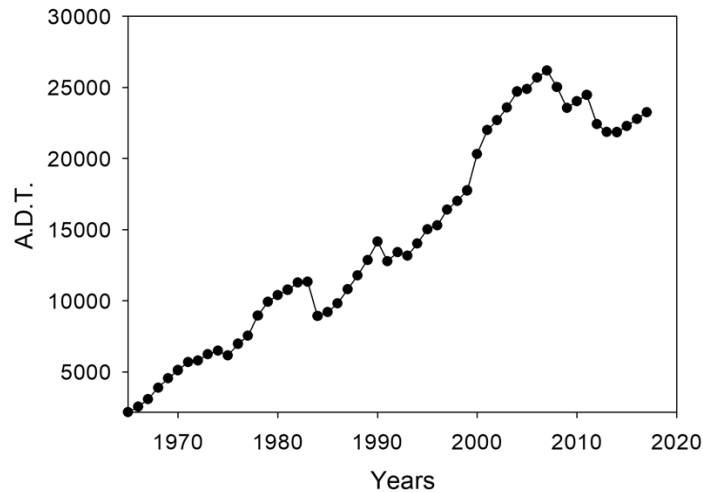


**Figure 9.** Truck ADT (AISCAT, 2019)

It is also of importance to consider the variability of the typical truck weights during the same time period (1968-2018). In the present study, the variation in truck weights from the mid-sixties to present date was estimated by employing the Italian design standards employed during the same period. For example, in the Guideline number 384 (1962) [28], which was employed during the design and construction of the Morandi Bridge, the total standard weight of a typical truck was

specified at 120 kN, at 40 kN for the front axle, and 80 kN for the rear axle (Fig. 10). These numbers have increased since then.

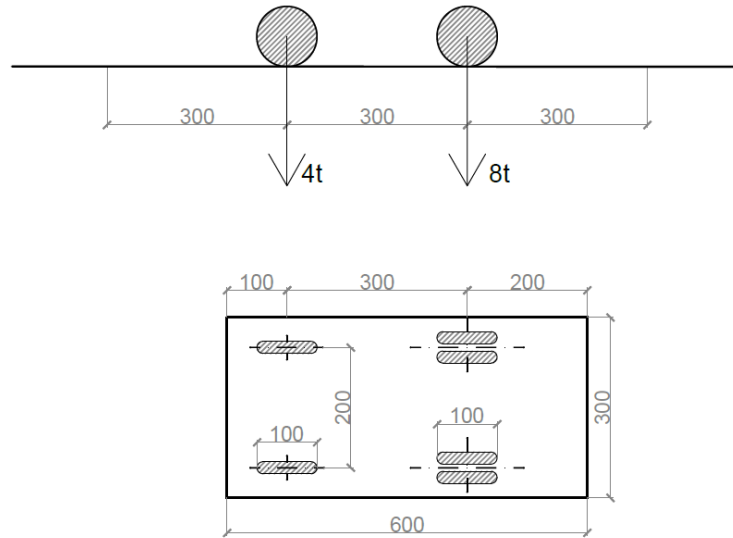


**Figure 10.** Design truck from Guideline number 384 (1962)

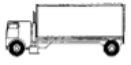


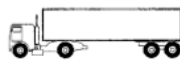

Accurate data pertaining to the exact types of trucks crossing the Morandi Bridge at the time of bridge failure was not available. However, there were no truck type limitations on the Polcevera Viaduct. Considering that A10 motorway serves as one of the pathways between Italy and the rest of the Europe via France, it was necessary to consider the entire range of European highway transit trucks for selection of the equivalent truck crossing over the bridge. Therefore, Table 1 based on the truck classification data in the Italian code, NTC-2018, was employed for determining the essential characteristics of the equivalent truck for the estimation of the live load on the bridge (2018). Data in Table 1 corresponds to the number of axles, axle weights, axle spacings, and percent share of traffic volume by the five truck types listed in the table. In particular, the number of axles ( $N_{Axles}$ ), axle weights ( $L_{Axles}$ ), and axle spacings ( $D_{Axles}$ ), of the equivalent truck were determined by computing the weighted average contribution of the five truck types with respect to the truck traffic composition ( $T_c$ ), as shown below:

$$N_{Axles} = \sum_1^5 (N_{Axles})_i \times (T_c)_i / \sum_1^5 (T_c)_i \approx 4 \quad (1)$$

$$D_{Axles} = \sum_1^5 (\bar{D}_{Axles})_i \times (T_c)_i / \sum_1^5 (T_c)_i \approx 3.32 \text{ m} \quad (2)$$

$$L_{Axles} = \left[ \sum_1^5 (L_{Truck})_i \times (T_c)_i / \sum_1^5 (T_c)_i \right] / N_{Axles} \approx 133.5 \text{ kN} \quad (3)$$

Where,  $\bar{D}_{Axles}$  is the average of axle spacings in individual trucks. The specifications for the equivalent truck based on the above-mentioned computations are provided in Fig. 11. A linear transition for variation in truck weights from 1968 to 2018 was assumed in the computation of the equivalent truck. This assumption was necessary for the computation of the change in the stresses exerted on the bridge components over the period of service. The change in axle numbers were based on the yearly changes in the number of axles per Italian codes. For the periods between 1968 to 1982, 1983 to 1998, and 1999 to 2018, the number of axles were 2, 3, and 4, respectively. The codes suggested use of variable numbers of axles in design, as shown in Table 1. from the computation of the equivalent truck, 4-axle we adopted in this study.

Truck type	Load [kN]	N° Axle	Axle Spacing [m]	% traffic composition
	280	2	4,2	20%
	360	3	2,75	5%
	630	5	2,75	50%
	560	4	3,73	15%
	610	5	3,52	10%

**Table 1.** Truck loads from NTC-2018



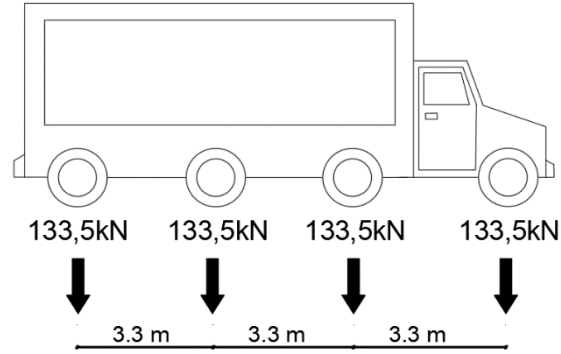


**Figure 11.** Equivalent average truck

## 6. Corrosion and Fatigue

In performing the capacity – demand analysis of the bridge, the effect of fatigue on the bridge capacity was computed based on the S-N curve, or Wöhler curve, of the stay cables (Fig. 8). The alternating stress,  $S$ , and the number of cycles,  $N$ , in the S-N curve were acquired from the equivalent truck axle weights for which their maximum effects on the bridge was computed through influence line analysis, and their yearly repeated action on the bridge per ADT data shown in Fig. 9. Corrosion affects both the capacity as well as the demand. On the capacity side, the combined effects of fatigue and corrosion lead to the degradation of the bridge and reduction of its capacity. Pitting corrosion was discovered in the cables of the Morandi Bridge following post collapse inspection of the cables [17]. Pitting corrosion creates localized holes and cavities in steel tendons. It is more destructive than uniform corrosion, and results in reduced capacity, especially under repeated loads. Pitting corrosion is also more difficult to detect, since its occurrence is local, subjecting the cables to high levels of stress concentration [29 - 32]. On the demand side, it has been experimentally demonstrated by Finozzi et al. (2018) that pitting corrosion reduces the ultimate and the yield strengths of steel [33]. Dai et al. (2016) has also shown that corrosion-induced damage is more pronounced in reducing the strength of prestressed concrete than the same in reinforced concrete structures [34]. Zhu, et al. (2015) presented the relationship between the stress concentration factor,  $\lambda$ , and the duration of the structure's exposure to corrosion for three different pitting geometries [35]:

$$\begin{cases} \lambda_r = 1,045 + 0,00335(t_1 - t_0) \\ \lambda_o = 1.039 + 0.00313(t_1 - t_0) \\ \lambda_t = 1.095 + 0.00234(t_1 - t_0) \end{cases} \quad (4)$$

Where,  $\lambda_r$  is for round pit,  $\lambda_o$  is for oval pit,  $\lambda_t$  is for triangular pit,  $t_0$  is initial service year and  $t_1$  is the current service year  $\lambda_r$  was employed for the computation of corrosion induced stress concentration, since the MIT report [17] indicated existence of severe pitting corrosion in the stays. The MIT report also indicates 20% corrosion induced mass loss in the cable. This was based on the assumption employed for retrofitting design of piers number 9 and 10 by a consulting firm for the management company of the bridge. As discussed in an earlier section of this article, estimation of capacity loss and increase in demand over the service life of the bridge was based on linear analysis. Hence, progression of corrosion in the cables of the bridge, from the time it was put to service, in 1968 to the time of collapse (1968 – 2018) was linearly back calculated from the twenty percent in 2018 to none, or zero percent, in 1968.

Xu et al. (2019) designed an experimental program in order to investigate the effect of corrosion on the mechanical properties of steel cables. Based on their investigations, a correlation relationship was developed between the mass loss due to corrosion and the yield and ultimate load proprieties of steel wires [36]. Their experimental research led to formulation of two linear relationships between the yield load ( $p_y$ ) and the ultimate load ( $p_u$ ) as a function of percent corrosion ( $\eta$ ):

$$p_y = 38,53 - 25,68 \cdot \eta \quad (5)$$

$$p_u = 40,18 - 27,86 \cdot \eta \quad (6)$$

In the present study, these relationships were employed in order to compute  $p_y$  and  $p_u$  as a function of percent corrosion in the cables of the Morandi bridge. In the computation of the yield and ultimate loads at various stages of corrosion, the following loss coefficients were herein introduced:

$$Y = \frac{p_y'}{p_y} \quad (7)$$

$$U = \frac{p_u'}{p_u} \quad (8)$$

Where,  $p_y'$  is the yield load at the current value of  $\eta$ , and  $p_y$  is the yield load in the absence of corrosion ( $\eta = 0\%$ ). Accordingly,  $p_u'$  is the ultimate load at the current value of  $\eta$ ,  $p_u$  is the ultimate load in the absence of corrosion ( $\eta = 0\%$ ).

By using Eqs. (7) and (8), the change in the mechanical properties of the steel cables due to percent corrosion induced mass loss,  $\eta$ , was computed. For example, Tables 2 and 3 correspond to the computed yield,  $\sigma_y$ , and ultimate,  $\sigma_u$ , strengths of steel cables at three different levels of corrosion, namely 0%, 8%, and 16% in 1968, 1988, and 2008, respectively.

**Table 2.** Computation of the change in yield strength due to corrosion

$\eta$	$p_y'$	$Y$	$\sigma_y$
[%]	[kN]	[%]	[MPa]
0	38,5	100	1450
8	36,5	94,7	1372,7
16	34,4	89,3	1295,4

**Table 3.** Computation of the change in ultimate strength due to corrosion

$\eta$	$p_u'$	$U$	$\sigma_u$
[%]	[kN]	[%]	[MPa]
0	40,2	100	1700
8	38,0	94,5	1605,7
16	35,7	88,9	1511,4

Corrosion weakens the fatigue strength by shifting the S-N curve down and to the left, lowering the number of cycles to failure within the applied level of stress range [37]. Corrosion induced weakening of fatigue strength in prestressing steel tendons has been investigated by a number of studies. For instance, Liu et al. (2017) developed an analytical relationship between the decrease in fatigue life and increase in corrosion of pre-stressing wires [38]. Lan, et al. (2018) also studied the corrosion induced weakening of the S-N curves for the stress range of 300 to 700 MPa in

parallel-wire stay cables [39]. Jiang et al. (2018) developed a model for corrosion induced degradation of S-N- $\eta$  surface of corroded steel wires in bridges [40]. Based on experimental evidence, they were able to formulate the relationships necessary to take into account the effect of corrosion in weakening of the S-N relations as follows [40]:

$$\begin{cases} \log(N) + (3.154 - 2.73\eta) \times \log(S) = 13.929 - 11.09\eta \\ \log(N) + (19.2461 - 96.16\eta) \times \log(S) = 55.1740 - 250.67\eta \end{cases} \quad (9)$$

Where, N is the number of cycles, S is the stress range and  $\eta$  is the percent corrosion in steel wires. Eq. (9) is valid for the stress range  $S \geq 360$  MPa, and Eq. (10) pertains for stress range,  $S < 360$ . In considering the deterioration of S-N curve for the tendons of the Morandi Bridge, Eqs. (9) and (10) were employed for development of S-N curves corresponding to each and every individual year of service beginning in 1968, corresponding to the yearly increase in percent corrosion, per earlier discussions. Typical S-N curves for the steel wires without corrosion (0%) in 1968, as well as those with 8 percent, and 16 percent corrosion induced mass losses in the subsequent years, respectively are shown in Fig. 12.

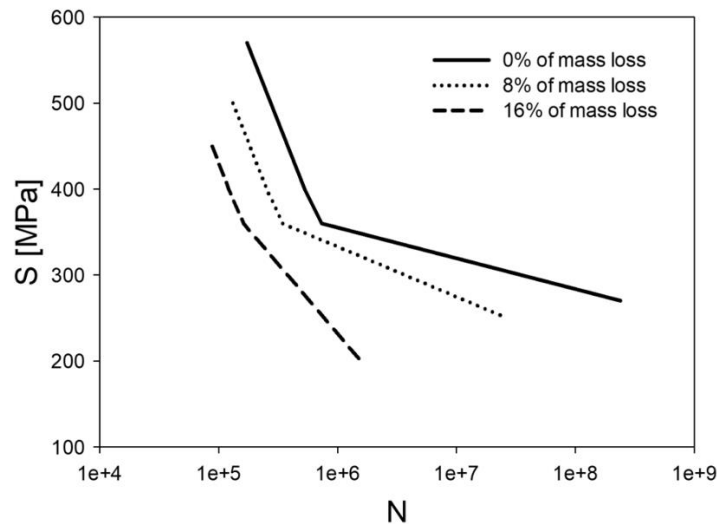


**Figure 12.** Typical S – N curves at 0%, 8% 16% of mass loss due to corrosion

## 7. Finite element model

A commercially available finite element (FE) program, SAP 2000 was employed for the development of the three-dimensional (3D) model and post collapse analysis of the bridge. 3D model of a typical pylon-deck system of the bridge is shown in Fig. 13. The original design tables, which were acquired from the Italian national state archives in Rome were employed for construction of the 3D model of the bridge segment [18, 19].

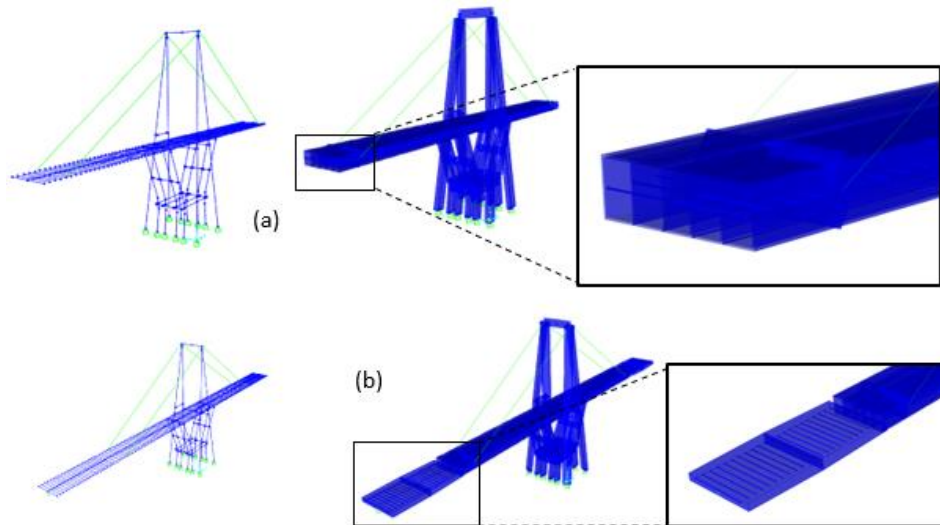


**Figure 13.** Finite Element model of the Deck-Pylon system (a): wireframe and solid model with detail of the cellular section. Complete model of the collapsed portion of the Polcevera viaduct (b): wireframe and solid model with detail of the Gerber systems.

The tower, the pier and the deck with the Gerber beams are modeled by using 399 *frame* elements, which were employed for representation of the beams, columns, braces, and truss elements in planar and 3D systems. The frame elements consist of linear segments, with a node on each side, accounting for biaxial bending, torsion, axial deformation, and biaxial shear in the beam-column formulation. The deck self-weight and added dead loads are carried by the cable stays and pylon, which were modeled as *frame elements*. Tendons A (352 strands) and B (112 strands) were modeled by *cable* elements, pretensioned with a force necessary to transform the bridge profile into the intended design shape following the release of the self-weight on the main girder. The concrete surrounding the stays were modeled by using a distributed load on the *cable* elements.

## Influence lines

The effect of moving loads on the major components of the bridge were determined by computing the influence lines. The classical approach by movement of a unit concentrated force across the bridge deck was employed for the computation of the influence lines. Axial force in cable stays, shear force in deck at pylon connection, shear force in deck at stay connection, and the reaction force at Gerber-support were identified as critical sections for analysis. Hence, the axles of the equivalent truck were placed on the critical sections identified by the influence lines, and for each case it was possible to figure out the truck position that created the maximum effect. The table style legends in Fig. 14 indicate the position of the truck axles and corresponding forces generated due to the position of the axle. For example, the maximum tension in the stay was obtained by placing the third axle of the truck on the critical section (Fig. 14a).

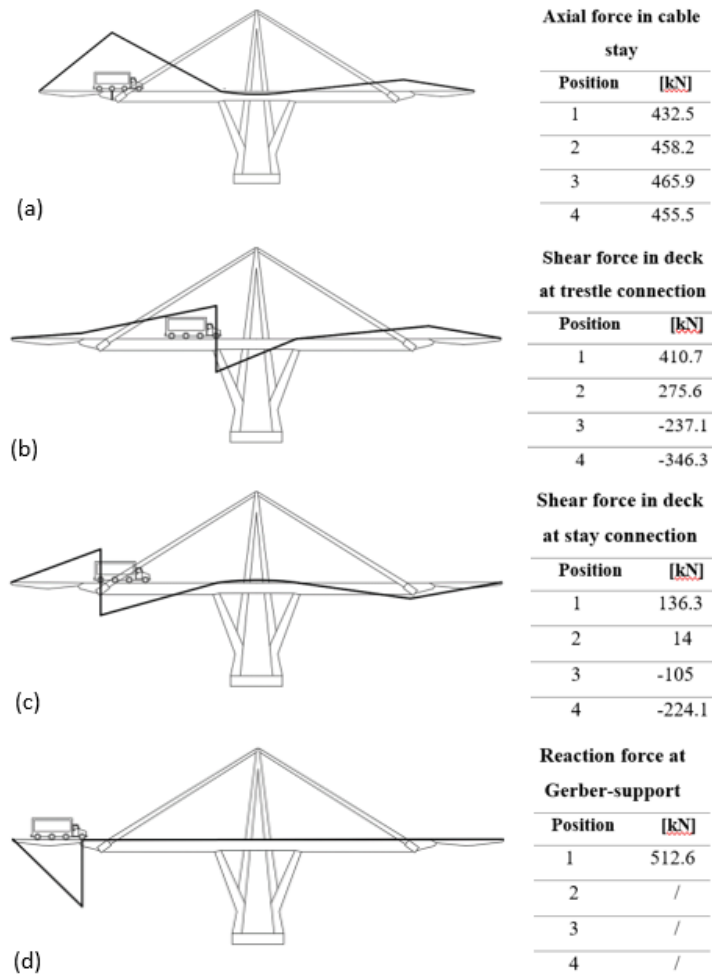


**Figure 14.** Influence lines: (a) axial force in cable stays, (b) shear force in deck at trestle connection, (c) shear force in deck at stay connection, (d) reaction force at Gerber-support

Considering the load path and the reaction influence line at the Gerber beam support in Fig. 14d, partial or full positioning of the truck axles on the Gerber beam would not affect the main girder of the bridge, even though it exerts a large load on the Gerber beam support. Therefore, the influence of the Gerber beam loads on the failure of girder-pylon system was discounted in the present study. Failure of the cable stay as indicated by the forces shown in Fig. 14a was considered as the main culprit for the collapse of the girder-pylon system.

## 8. Cumulative Damage

S-N curves are usually generated at constant amplitude loading conditions. However, real structures as the Morandi bridge are subjected to different stress range and, therefore, their fatigue life prediction has to be studied using a more consistent approach. In this study, the Palmgren-Miner-law was employed for estimating the remaining life of the bridge subjected to fatigue loads. Considering variable load history and a cumulative damage to predict the fatigue life of the stay tendons, Palmgren-Miner-law is written in the following form:

$$\sum_{i=1}^k \frac{n_i}{N_i} = 1 \quad (11)$$

Where,  $k$  is the number of stress levels in the block loading spectrum, and  $n_i$  and  $N_i$  are the number of cycles applied and the fatigue life at  $S_i$ , respectively,  $S_i$  being the  $i$ -th stress level. The stress range and the stress amplitude per year were computed as follows:

$$\tilde{S}_i = \phi \cdot \lambda_r \cdot \Delta\sigma \quad (12)$$

$$S_i = \frac{\tilde{S}_i}{2} \quad (13)$$

Where,  $S_i$  is the stress amplitude,  $\tilde{S}_i$  is the stress range,  $\phi = 1.4$  is the dynamic amplification factor from Eurocode 1 Annex B [41],  $\lambda_r$  is the stress concentration factor due to round pitting corrosion by Eq. (4) and  $\Delta\sigma$  is the difference in stress given by the truck.  $S_i$  in each year was computed by eq. (13) and substituted in Eq. (10) to obtain the fatigue life  $N_i$ .

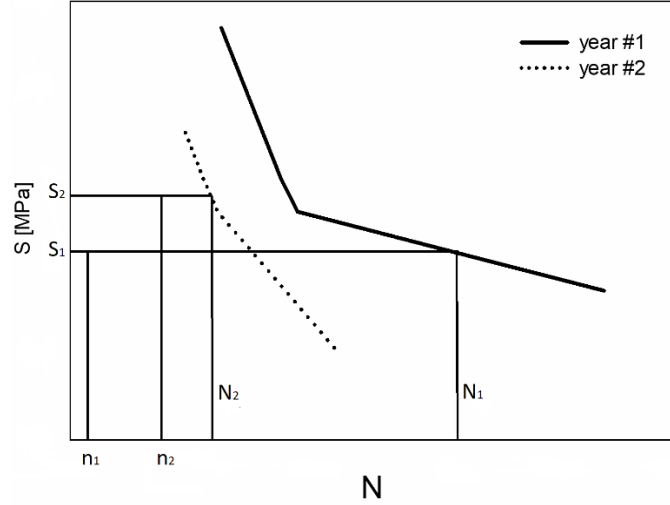


**Figure 15.** Component cyclic life determined from Palmgren-Miner law

Estimation of the remaining life of the bridge was computed individually for every year of service over total service period of,  $k$ , years accordingly:

$$D = 365 \times \left[ \frac{n_1}{N_1} + \frac{n_2}{N_2} + \dots + \frac{n_k}{N_k} \right] \quad (14)$$

$$R = 1 - D \quad (15)$$

$$d \times \left[ \frac{n_1}{N_1} + \frac{n_2}{N_2} + \dots + \frac{n_k}{N_k} \right] = R \quad (16)$$

Where,  $D$  is the amount of damage,  $R$  is the remaining fatigue life,  $d$  is the remaining days of service life,  $n_k$ , is the ADT, and once multiplied by 365 yields the total number of cycles per year at  $S_i$ , and  $N_i$  is the fatigue life at  $S_i$ . As an example, in Fig. 15, for year 1,  $N_1$  was computed inserting  $S_1$  in Eq. 10. Then,  $N_2$  was computed in the same manner by using,  $S_2$ . The total amount of damage,  $D$  at year 2 was then computed by Eq. 14 as:

$$D = 365 \times \left[ \frac{n_1}{N_1} + \frac{n_2}{N_2} \right] \quad (17)$$

Then, the remaining fatigue life,  $R$ , after years 1 and 2 was computed by Eq. 15, and the remaining days of service life were computed from Eq. 16 as follows:

$$d \times \left[ \frac{n_1}{N_1} + \frac{n_2}{N_2} \right] = R \quad (18)$$



Repeating this procedure for every year of bridge service life since its inception, it was possible to compute the remaining days of service life per year as shown in Fig. 16. It is possible to observe as tendons B reach failure in 2013 and tendons A fail in 2014, leading to total collapse. The cumulative damage model based on Palmgren-Miner-law predicted the collapse date of the Morandi bridge 4 years earlier than the actual collapse date of 2018.

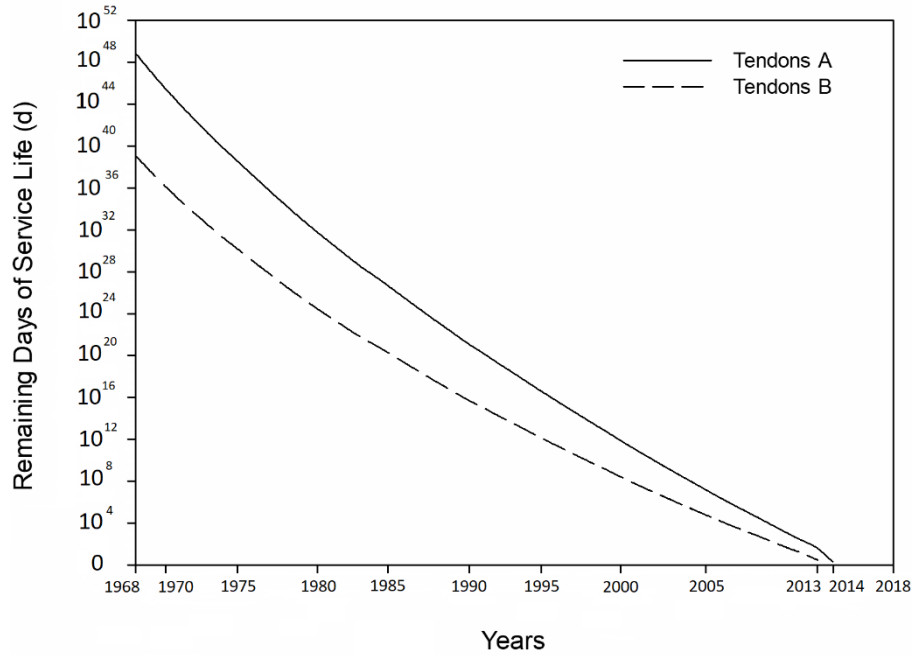


**Figure 16.** Remaining days of service life Tendons A and Tendons B.

### 9. Effect of Mean Stress on Fatigue Life

In the evaluation of material's fatigue response, it is important to consider the mean stress,  $S_m$ , because increasing  $S_m$ , leads to decrease in fatigue life for a given alternating stress amplitude,  $S_a$  [42]. In essence, it is important to estimate the fatigue life of the bridge based on the amplitude of mean cyclic stress, in relation to the material's tensile strength. A number of analytical relationships have been developed in order to determine the effect of mean stress on the fatigue life of the materials, including the empirical relationships developed by Goodman, Gerber, and Soderberg as follows:

$$S_a = \sigma_{fat} \left( 1 - \frac{S_m}{\sigma_{ts}} \right) \quad (19) \quad \text{Goodman}$$

$$S_a = \sigma_{fat} \left[ 1 - \left( \frac{S_m}{\sigma_{ts}} \right)^2 \right] \quad (20) \quad \text{Gerber}$$

$$S_a = \sigma_{fat} \left( 1 - \frac{S_m}{\sigma_{ys}} \right) \quad (21) \quad \text{Soderberg}$$

Where,  $S_a$  is the alternating stress amplitude,  $S_m$  is the mean stress,  $\sigma_{fat}$  is the fatigue strength,  $\sigma_{ts}$  is the tensile strength and  $\sigma_{ys}$  is the yield strength. The graphical representation of these empirical relationships, namely Goodman, Gerber, and Soderberg diagrams provide the limiting surface in  $S_a$ - $S_m$  domain, within the tensile strength limits of the material. In terms of fatigue life, Goodman and Soderberg provide more conservative results than Gerber. These relationships were employed in the current study, in order to compare the rationality of the various approaches for estimating the remaining life of the stay cables of the Polcevera viaduct.

In Eqs. (19), (20), and (21),  $\sigma_{fat}$  is computed by using Eq. (10), and setting  $N$ , the number of cycles to  $2 \times 10^6$  pertaining to the endurance limit of the test specimen per PTI [43], fib [44], and SETRA [45]. The effect of corrosion on  $\sigma_{fat}$  was considered by increasing  $\eta$  for the individual years of service in Eq. (10).  $S_m$  was similarly computed for individual years of service by using the following relationships:

$$\tilde{S}_i = \phi \cdot \lambda_r \cdot \Delta\sigma \quad (22)$$

$$\sigma_{min} = \sigma'_{min} \cdot \lambda_r \quad (23)$$

$$\sigma_{max} = \sigma_{min} + S_i \quad (24)$$

$$S_m = \frac{\sigma_{max} + \sigma_{min}}{2} \quad (25)$$

Where,  $\tilde{S}_i$  is the stress range,  $\phi = 1.4$  is the dynamic amplification factor from Eurocode 1 Annex B [41],  $\lambda_r$  is the stress concentration factor due to round pitting corrosion from Eq. (4),  $\Delta\sigma$  is

the difference in stress given by the truck,  $\sigma'_{\min}$  is the stress in the tendons due to dead load,  $\sigma_{\min}$  is the stress in the tendons due to the combination of dead load and corrosion,  $\sigma_{\max}$  is the stress in the tendons due to the sum of dead load and the moving load,  $S_m$  is the mean stress. It is then possible to plot the Goodman, Gerber, and Soderberg diagrams for individual years of service for the stay cables as the bridge deteriorates due to corrosion and fatigue.

Fig. 17 corresponds to the Goodman, Gerber, and Soderberg diagrams for the years 2013, and 2014, respectively, the years in which tendons B, and A failed based on the cumulative damage computations of Palmgren-Miner-law. Comparison of the results shown in Fig. 17 reveals the contrast between the timing of stay cable failure predicted by the Palmgren-Miner-law, and the Goodman, Gerber, and Soderberg diagrams. According to these diagrams, the bridge would not collapse in 2014, as predicted by the cumulative damage model. However, As shown by the Gerber, and Goodman diagrams in the subsequent years, shown in Fig. 18, the stay cables A and B fail in 2015, and 2016, respectively. The stay cables would have still remained in service by the Soderberg  $S_a$ - $S_m$  law, which is less conservative than its counterparts (Gerber, and Goodman).

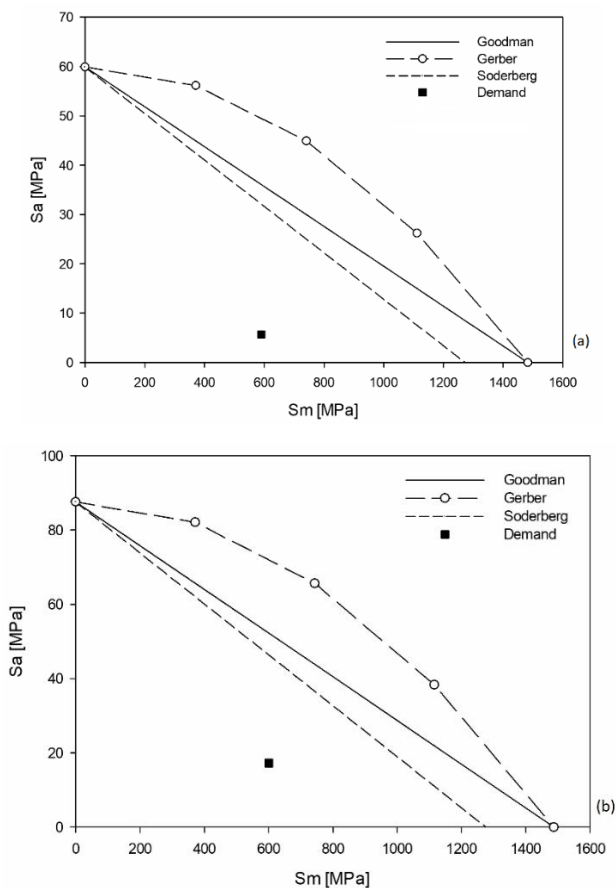


**Figure 17.** Goodman, Gerber and Soderberg surface (a) Tendons A in 2014, (b) Tendons B in 2013.

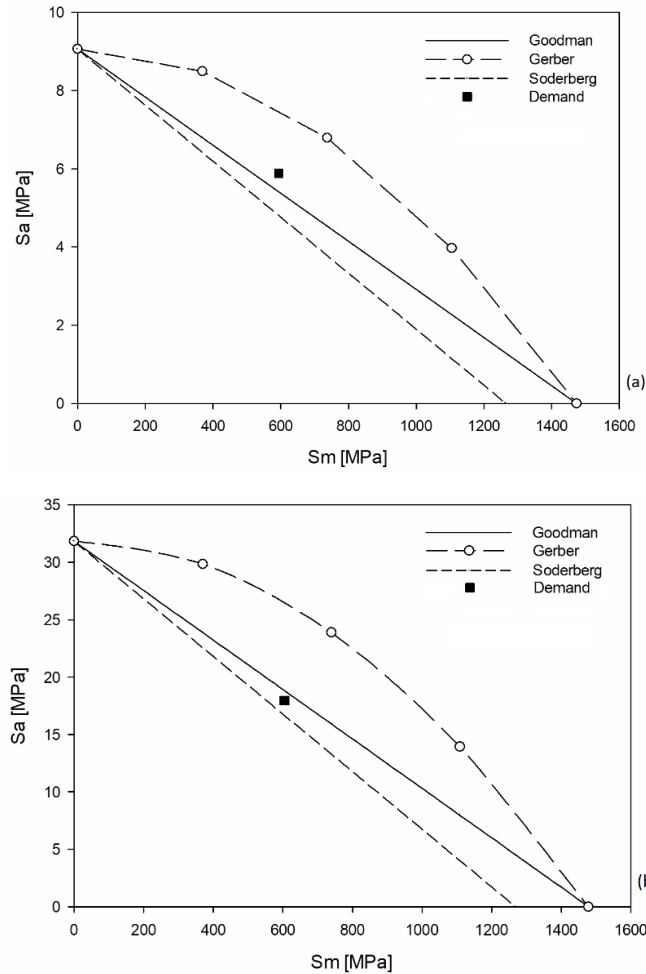


**Figure 18.** Goodman, Gerber and Soderberg surface (a) Tendons A in 2016, (b) Tendons B in 2015.

Considering that the actual collapse of the bridge occurred in 2018, one may consider the results of this study satisfactory. However, this study was based on collection of available corrosion and fatigue models and estimates of archival traffic data. Survey of literature during the course of this study revealed lack of sufficient information about corrosion and fatigue models for steel cable tendons. Therefore, the corrosion-fatigue model employed in this study needs to be further studied by more experimental data for statistical viability. Other simplifying assumptions made during the service life of the bridge were linearization of degradation due to corrosion and increase in

traffic from the time of its inception in 1968 till the time of its collapse. Nevertheless, the method presented in this study provides a holistic approach for estimating the service life of bridges when sensor-based methods are unavailable.

## **10. Conclusions**

The study reported in this article aimed at estimating the remaining service life, or to predict the timing of the collapse of the Morandi Bridge, considering the information available at the time of this writing. Ideally, the best approach was by sensor based real time structural health monitoring of the bridge. In lieu of instrumented methods, the work presented in this study employed the existing knowledge in estimating the remaining life of the bridge, including: the existing design information about the bridge; post collapse investigation report of the ministry of infrastructure and transport [17]; and archival truck traffic and axle load data.

The design had features that were characteristically different from conventional methods, such as the fact that the individual pylon-deck systems of the bridge were only supported by two stays on each side running over the pylons over saddle seats. This design did not allow for redundancy, especially when the stay cables were made of prestressed concrete and difficult to inspect for corrosion. Nevertheless, the bridge lasted for over 50 years, without much maintenance, especially at the cable stays, except at one of the pylons, which did not collapse (P 11 in Fig. 3).

The post collapse analysis of the bridge involved time-domain estimation of bridge capacity loss over the period of bridge service and increase in demand over the same period (1968 – 2018). The existing information about the bridge was employed together with pertinent corrosion and fatigue models to estimate the decrease in the capacity of the bridge from the time it was placed in service. The archival load and traffic data were employed together with the design codes, dating back to the time the bridge constructed until the present time, in order to estimate the increase in demand for the bridge during its service life. Classical influence line analysis of the individual sections of the pylon-deck system of the bridge, together with the finite element model of the bridge provided the numerical tool for analysis of the bridge.

A number of different approaches were compared in estimating the remaining life of the bridge, including the cumulative damage law of Palmgren-Miner-law, and the Goodman, Gerber and Soderberg  $S_a$ - $S_m$  diagrams. The predicted timing of collapse by these models ranged from the year 2014 based on the cumulative damage law, and 2016 by the Gerber and Goodman diagrams.

Results from this study suggest collapse of the bridge 2-4 years prior to the actual collapse date in 2018. This study involved only numerical analysis based on limited amount of information about the condition of the bridge. It was based on the hypothesis considering the combination of fatigue and corrosion of the cable stays as the main factor leading to the partial collapse of the bridge. The study employed the limited amount of information about the corrosion – fatigue models available in the technical literature to perform the analysis. Selection of other available models could have changed the outcome of this study, perhaps by a couple of years prior or after the actual date, or the estimations made in the present study. Nevertheless, such studies provide valuable predictions of service life estimates that could be used in planning for preventive maintenance of structures. The fundamentals of the approach taken herein, are realistic considering the basic principle of demand surpassing the capacity in terms of progressive change in the condition of the bridge and its traffic patterns.

It is true that this bridge defied the current principles of design and construction methods. However, despite the unusual design features and lack of redundancy, the bridge lasted for fifty years, without much efforts in the maintenance of the cable stays. Certainly, real time condition monitoring of the bridge would have made a major difference in preventing the partial collapse of the bridge. The results of this study indicated that even without an active instrumented structural health monitoring system, basic engineering principles may provide the backing for estimation of remaining life of the infrastructure. In the case of the Morandi bridge, such an analysis at some point during its service life, would have possibly predicted imminence of collapse prior to the actual collapse.

## **11. Acknowledgements**

The research funding by the European Research Council under the Grant Agreement n°ERC\_IDEalreSCUE\_637842 of the project IDE-AL RESCUE - Integrated Design and control of Sustainable CommUnities during Emergencies is greatly appreciated. Alessandro Zona performed some numerical analyses in partial fulfilment for the requirements of the Bachelor's Degree in Civil Engineering at Politecnico di Torino, under the guidance of the Authors. His contribution is gratefully acknowledged.

## 12. References

1. Ansari F (2005) Fiber optic health monitoring of civil structures using long gage and acoustic sensors. *Smart Materials & Structures* 14(3): S1-S7
2. Zarafshan A, Iranmanesh A, Ansari F (2012) Vibration-Based and Sensor for Monitoring of Bridge Scour. *Journal of Bridge Engineering* 17(6): 829-838
3. LeRose C (2001) The Collapse of the Silver Bridge West Virginia. *Historical Society Quarterly*. **15** (4)
4. Lichtenstein AG (1993) The Silver Bridge Collapse Recounted. ASCE , *Journal of Performance of Constructed Facilities*, Vol.7, No. 4, [https://doi.org/10.1061/\(ASCE\)0887-3828\(1993\)7:4\(249\)](https://doi.org/10.1061/(ASCE)0887-3828(1993)7:4(249))
5. Salem HM, Helmy HM (2014) Numerical investigation of collapse of the Minnesota I-35W bridge. *Engineering Structures*, Vol.59, pp. 635-645
6. National Transportation Safety Board (NTSB) (2008) Collapse of I-35W highway bridge, Minneapolis, Minnesota, August 1, 2007. Highway Accident, Report NTSB/HAR-08/03
7. Beshah F, Wright W, and Graybeal B, (2008) I-35W over the Mississippi River. Federal Highway Administration Turner Fairbank Highway Research Center Report
8. Lee SB (1996) Fatigue failure of welded vertical members of a steel truss bridge. *Eng. Fail. Anal.*, 3(2), 103–108
9. National Transportation Safety Board (NTSB) (1984) Collapse of a Suspended Span of Interstate Route 95 Highway Bridge over the Mianus River, Greenwich, Connecticut, June 23, 1983. Highway Accident, Report PB84-916203
10. Deng L, Wang W, Yu Y (2016) State-of-the-Art Review on the Causes and Mechanisms of Bridge Collapse. ASCE, *Journal of Performance of constructed Facilities*, Vol. 30, No.2
11. Choudhury JR, Hasnat A, (2015) Bridge collapses around the world: Causes and mechanisms. IABSE-JSCE Joint Conference on Advances in Bridge Engineering-III, August 21-22, 2015, Dhaka, Bangladesh, Amin, Okui, Bhuiyan, Ueda (eds.), ISBN: 978-984-33-9313-5
12. Talebinejad I, Fischer C and Ansari F (2011) Numerical Evaluation of Vibration-Based Methods for Damage Assessment of Cable-Stayed Bridges. *Computer-Aided Civil and Infrastructure Engineering* **26**(3): 239-251
13. Oskoui EA, Taylor T and Ansari F (2019) Method and monitoring approach for distributed detection of damage in multi-span continuous bridges *Engineering Structures* **189**: 385-395

14. Nazarian E, Ansari F, Zhang XT and Taylor T (2016) Detection of Tension Loss in Cables of Cable-Stayed Bridges by Distributed Monitoring of Bridge Deck Strains. *Journal of Structural Engineering* **142**(6)
15. AASHTO LRFD Bridge Design Specifications, 8<sup>th</sup> Edition, September 2017, LRFD-8, ISBN: 978-1-56051-654-5
16. Fabrizio Gatti (2018) Ponte Morandi, le foto shock prima del crollo: travi rotte e cavi ridotti del 75 per cent. *L'Espresso* <http://espresso.repubblica.it/attualita/2018/09/13/news/ponte-morandi-1.326939>, Accessed June 17, 2019
17. Ministero delle Infrastrutture e dei Trasporti, Commissione Ispettiva Ministeriale, “Comune di Genova, Autostrada A10 – Crollo del Viadotto Polcevera, Evento Accaduto il 14 Agosto 2018”, 14 Settembre 2018, Roma. Available online: <http://www.mit.gov.it/comunicazione/news/ponte-crollo-ponte-morandi-commissione-ispettiva-genova/ponte-morandi-online-la> Accessed June 17, 2019
18. Morandi R (1967) Il viadotto sul Polcevera per l'autostrada Genova-Savona. *L'Industria Italiana del Cemento*, XXXVII:849–872
19. Morandi R (1968) Viaducto sobre el Polcevera, en Génova Italia. *Informes de la Construcción*, 21(200)
20. Domaneschi M, Cimellaro GP, Scutiero G (2018) Disproportionate collapse of a cable-stayed bridge. *Proceedings of the Institution of Civil Engineers - Bridge Engineering* 172(1):13-26. DOI: 10.1680/jbren.18.00031
21. Nazarian E, Ansari F and Azari H (2016) Recursive optimization method for monitoring of tension loss in cables of cable-stayed bridges. *Journal of Intelligent Material Systems and Structures* 27(15): 2091-2101
22. Scarella, A, Salamone G, Babanajad SK, De Stefano A and Ansari F (2017) Dynamic Brillouin Scattering-Based Condition Assessment of Cables in Cable-Stayed Bridges. *Journal of Bridge Engineering* 22(3)
23. Vairo T, Quagliati M, Pagani E., Beggiato M, Lantero A, Della Penna R, Vestri G (2012) Determinazione del contributo dell'aerosol marino alla frazione PM10 sulla costa ligure. *Convegno Nazionale sul Particolato Atmosferico*, 16-18 May 2012, Perugia, Italy



24. Vairo T, Quagliati M, Pagani E., Bertolotto M, Beggiato M, Vestri G (2014) La dispersione atmosferica di aerosol marino dalla costa verso l'interno. Convegno Nazionale sul Particolato Atmosferico, 20-23 Maggio 2014, Genova, Italy
25. Calvi GM, Moratti M, O'Reilly GJ, Scattarreggia N, Monteiro R, Malomo D, Calvi PM, Pinho R (2019) Once upon a Time in Italy: The Tale of the Morandi Bridge. *Structural Engineering International*, 29(2): 198-217
26. Lu N, Noori M, Liu Y (2017) First-passage probability of the deflection of a cable-stayed bridge under long-term site-specific traffic loading. *Advances in Mechanical Engineering*, 9(1):1–10. DOI: 10.1177/1687814016687271
27. AISCAT - Associazione Italiana Società Concessionarie Autostrade e Trafori (2019), <http://www.aiscat.it/>, Accessed July 17, 2019
28. Ministero dei Lavori Pubblici (1962) Norme relative ai carichi per il calcolo dei ponti stradali. Guideline nr. 384
29. BaniAsad, Dehestani E and Dehestani M (2019) Incorporation of corrosion and bond-slip effects in properties of reinforcing element embedded in concrete beams. *Structures* **20**: 105-115
30. Baumgartner A, Fraundorfer A, Dauberschmidt C and Kustermann A (2019) Influence of chloride induced pitting corrosion on the mechanical properties of reinforcing bars. *Beton-Und Stahlbetonbau* **114**(6): 409-418
31. Guo X, Situm A, Barlow BC, Guo B, Burgess IJ and Grosvenor AP (2019) Soft X-ray spectromicroscopy studies of pitting corrosion of reinforcing steel bar. *Surface and Interface Analysis* **51**(6): 681-691
32. Wu Q, Li X, Xu J, Wang G, Shi W and Wang S (2019) Size Distribution Model and Development Characteristics of Corrosion Pits in Concrete under Two Curing Methods. *Materials* **12**(11).
33. Finozzi I, Saetta A, Budelmann H (2018) Structural response of reinforcing bars affected by pitting corrosion: experimental evaluation. *Construction and Building Materials*, 192: 478-488.
34. Dai L, Wang L, Zhang J, Zhang X (2016) A global model for corrosion-induced cracking in prestressed concrete structures. *Engineering Failure Analysis* 62:263-275

35. Zhu J, Huang F, Guo T and Song Y (2015) Residual life evaluation of prestressed reinforced concrete highway bridges under coupled corrosion-fatigue action. *Advanced Steel Construction* Vol.11, No 3, pp. 372-382
36. Xu F, Chen Y, Zheng X, Ma R and Tian H (2019) Experimental study on corrosion and mechanical behavior of main cable wires considering the effect of strain. *Materials* 2019, 12, 753; doi:10.3390/ma12050753
37. Adasooriya ND, Hemmingsen T, and Pavlou D (2017) Fatigue strength degradation of metals in corrosive environments. *IOP Conf. Series: Materials Science and Engineering* 276 (2017) 012039.
38. Liu X, Zhang W, Gu X, Zeng Liu Y et al. (2017) Degradation of Mechanical Behavior of Corroded Pre-stressing Wires Subjected to High-Cycle Fatigue Loading. *Journal of Bridge Engineering*, 22(5).
39. Lan C, Xu Y, Liu C, Li H, Spencer BF Jr (2018) Fatigue life prediction for parallel-wire stay cables considering corrosion effects. *International Journal of Fatigue*, 114: 81-91.
40. Jiang C, Wu C, Jiang X (2018) Experimental study on fatigue performance of corroded high-strength steel wires used in bridges. *Construction and Building Materials*, 187: 681-690.
41. Comité Europeo de Normalizacion (CEN) (2003), Eurocode 1: Actions on structures – Part 2: Traffic loads on bridges. EN 1991-2
42. Hertzberg RW, Vinci RP, Hertzberg JL (2012) *Deformation and Fracture Mechanics of Engineering Materials*. Wiley, USA.
43. Post Tensioning Institute (PTI). “PTI Guide Specification. Recommendations for stay cable Design, Testing and installation”, 2007
44. Federation internationale du beton (fib). “Bulletin 30 Acceptance of stay cable systems using prestressing steel”, 2005
45. SETRA Cable Stays Recommendations of French Interministerial Commission on Prestressing. “Haubans – Recommendations de la CIP”, 2022